ELSEVIER

Materials Science and Engineering A351 (2003) 183–189

MATERIALS SCIENCE & ENGINEERING A

www.elsevier.com/locate/msea

Determination of microstructural criterion for cryogenic toughness variation in actual HAZs using microstructure-distribution maps

Jae-il Jang [a,*], Jung-Suk Lee [b], Jang-Bog Ju [b], Baik-Woo Lee [b], Dongil Kwon [b], Woo-Sik Kim [c]

[a] *Frontics, Inc., Research Institute of Advanced Materials, Seoul National University, Seoul 151-742, South Korea*
[b] *School of Materials Science and Engineering, Seoul National University, Seoul 151-742, South Korea*
[c] *Research and Development Center, Korea Gas Corporation, Ansan 425-150, South Korea*

Received 10 December 2001; accepted 28 October 2002

Abstract

It is well known that heat-affected zone (HAZ)-notched fracture mechanics tests, such as crack tip opening displacement (CTOD) test, are very sensitive to the microstructural gradient in the HAZ. This study aimed to investigate the distribution of microstructures, including local brittle zones (LBZs), in the actual HAZ of advanced 9% Ni cryogenic steel, and to determine a microstructure criterion for the change in cryogenic toughness of the steel HAZs using microstructure-distribution maps. To estimate the microstructural influence more systematically, K-grooved HAZ specimens were prepared. Analysis using these microstructure-distribution maps constructed from the specimens tested at 111 K revealed that the weakest-link-type fracture occurs mainly in regions having a large fraction of LBZs (over 17%), whereas the fracture toughness of the other regions was found to be governed by a mixture-rule of the microstructures existing at the precrack tip front of CTOD specimen.

Keywords: Weld; Heat-affected zone (HAZ); Microstructure-distribution map; Fracture toughness; Local brittle zone (LBZ); 9% Ni steel

1. Introduction

The excellent toughness of quenching, lamellarizing and tempering (QLT)-processed 9% Ni steel, recently developed for large-scale liquefied natural gas (LNG) storage tanks [1], at cryogenic temperatures such as 111 K of LNG temperature can be upset during multi-pass welding procedures because, as is well known, toughness values are very sensitive to microstructural change within heat-affected zones (HAZs). Thus a correlation of the weld thermal cycles with microstructures is very important in understanding fracture mechanisms in welded joints.

In the authors' previous studies [2,3], microscopic fracture behavior of the HAZs in this steel was observed on simulated HAZ specimens. This work revealed that the advanced 9% Ni steel has local brittle zones (LBZs), i.e. small zones of abnormally low fracture toughness, like other high-strength structural steels [4–6]. Furthermore, intercritically reheated coarse-grained HAZ (IC CGHAZ) and unaltered coarse-grained HAZ (UA CGHAZ) are the primary and secondary LBZs of this steel, respectively, at cryogenic temperatures. Although these results provided valuable insights into the microscopic fracture mechanism and the existence of weak zones within the HAZs, they remain inadequate to give practical information on the overall relationship between the distribution of subregions having different microstructures and HAZ toughness in actual weld joints. Continuing this line of research, therefore, the present work was undertaken to analyze the influence of microstructure distribution on cryogenic toughness variation in actual welded joints and to determine a microstructural criterion for the change in fracture mechanism. For systematic evaluation, K-grooved HAZ specimens were used for the toughness tests such as crack tip opening displacement (CTOD) tests and

* Corresponding author. Present address: Metals and Ceramics Division, Oak Ridge National Laboratory, PO Box 2008, Oak Ridge, TN 37831-6136, USA. Tel.: +1-865-574-5357; fax: +1-865-576-5413.
E-mail address: jijang@frontics.com (J.-i. Jang).

0921-5093/03/$ - see front matter
PII: S0921-5093(02)00850-X

Charpy impact tests. Microstructure-distribution maps were constructed from the CTOD specimens, and were used for more quantitative investigation.

2. Experimental

The composition and basic mechanical properties of the material used in this study are given in Table 1. The steel is a commercial grade used for LNG storage tanks in Korea. The plates are normally processed by the QLT heat treatment: Q (1093 K for 60 min, quench), L (963 K for 80 min, quench) and T (853 K for 60 min, quench).

The steel plates of 22 mm thickness (the thickness of the largest of the inner walls of Korean LNG storage tanks) were machined into a K-groove configuration as shown in Fig. 1. They were welded along the transverse-to-rolling direction either by shielded metal arc welding (SMAW) or submerged arc welding (SAW) under the same conditions as used during the construction of the tanks in Korea, as listed in Table 2. No significant defects in the completed weld joints were found in non-destructive radiographic examination.

CTOD tests were conducted mainly in accordance with ASTM E1290 [7] at cryogenic temperatures such as LNG temperature (i.e. 111 K). Fig. 2 is a schematic view of the testing apparatus and the geometry of CTOD specimens used in this study. The through-thickness precracks were located at various distances from the fusion line (FL), as shown in Fig. 3. When calculating the CTOD values from the crack mouth opening displacement (CMOD) data, the asymmetry of plastic deformation around the crack tip was taken into consideration using the "local CTOD" approach [8,9], because the weld joints used in this study had strength mismatches between the austenitic weld metal (Inconel or Hastelloy alloy) and the ferric base metal. In addition, uniform fatigue precracks in the test specimens, which have been an issue in weldment fracture toughness tests, were carefully induced according to the "partial arc notching method" developed in a previous study [10]. The tested specimens were examined to ensure that the precrack location was within the region of interest.

Table 1
Chemical composition and mechanical properties of QLT-9% Ni steel

Chemical compositions (wt.%)	
C	0.066
Si	0.24
Mn	0.65
P	0.005
S	0.005
Ni	9.28
Mechanical properties at RT/at 77 K	
YP (MPa)	640/910
TS (MPa)	710/1140
EL (%)	36/34

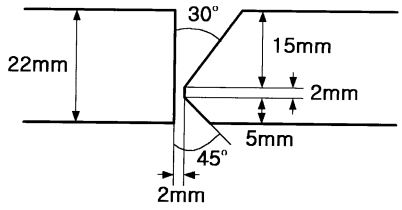

Fig. 1. Schematic view of K-grooved weld joint preparation.

To verify the tendency of toughness changes seen in the CTOD tests, Charpy impact tests were additionally performed at low temperatures. Standard 2 mm V-notched specimens were taken from the center of thickness in the K-grooved weld joints, and the notch positions from FL are the same as in Fig. 3. In both CTOD tests and Charpy impact tests, at least three toughness values were obtained from the tests under each condition, and only the minimum of the values was used to estimate the lower bound toughness.

3. Results and discussion

Fig. 4 shows the results of CTOD tests at low temperatures using SMA- and SA-welded HAZ specimens with K-grooves. HAZ fracture toughness, represented by the CTOD values, peaks at the FL+2 mm and decreases as the precrack location approaches FL from the base metal. Charpy impact tests show that the impact energy variation along the distance from FL exhibits a similar trend to CTOD values as shown in Fig. 5.

To evaluate systematically the influence of the microstructure distribution in the fatigue precrack tip on cryogenic HAZ fracture properties, a schematic diagram of thermal cycle history and microstructures, called a microstructure-distribution map, was constructed for each specimen by the method detailed below.

First, sectioning of the specimen tested at LNG temperature, 111 K, was carried out in the manner recommended by API RP 2Z [11], as shown schematically in Fig. 6. Polishing and macroscopic 5%-Nital-etching were performed sequentially, and then the thermal cycle history was indicated on the surface of the specimens, as shown in Fig. 7, using the following equation (generally used for explaining the thermal cycle range according to peak temperature [12,13]):

$$\frac{r}{d_{\mathrm{HAZ}}} = \frac{\sqrt{A_{\mathrm{C3}} - T_0}}{\sqrt{T_{\mathrm{p}} - T_0}} \times \frac{\sqrt{T_{\mathrm{mp}} - T_0} - \sqrt{T_{\mathrm{p}} - T_0}}{\sqrt{(T_{\mathrm{mp}} - T_0) - \sqrt{(A_{\mathrm{C3}} - T_0)}}}, \quad (1)$$

where r is the perpendicular distance from FL to the region with peak temperature (T_{p}), T_{mp} the melting

Table 2
Welding conditions used in this study

Welding method	Welding materials (type)	Polarity	Inter-pass temperature (K)	Current (A)	Voltage (V)	Speed (cm min^{-1})	Average heat input (kJ cm^{-1})
SMAW (vertical)	Hastelloy	AC	383	100–130	20–40	6–20	28
SAW (flat)	Inconel	DCEP	423	320–360	25–28	25–53	23

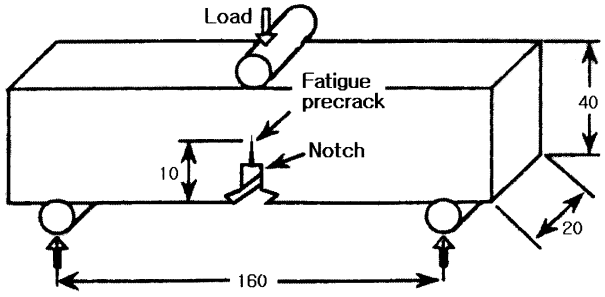

Fig. 2. Schematic illustration of CTOD test set-up and specimen geometry.

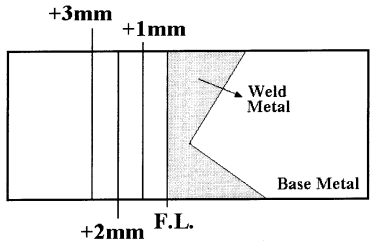

Fig. 3. Schematic diagram showing notch locations in CTOD tests and Charpy impact tests.

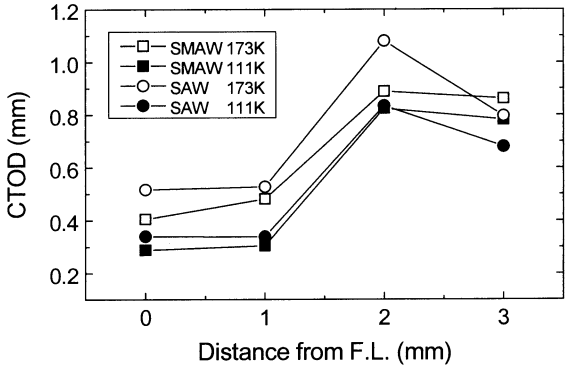

Fig. 4. Variations in CTOD values with distance from FL.

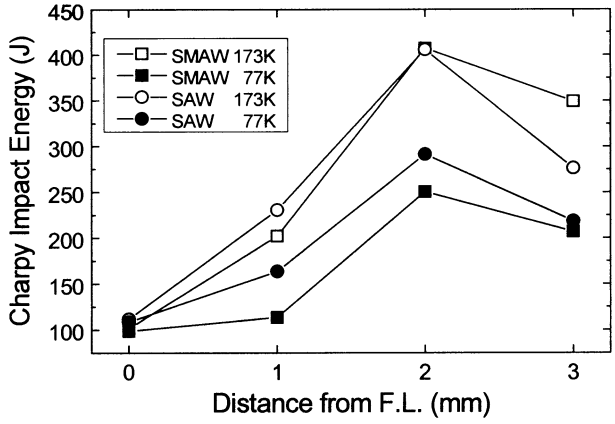

Fig. 5. Variations in Charpy impact values with distance from FL.

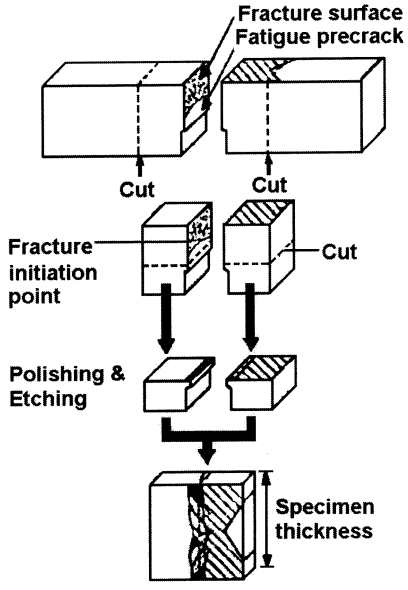

Fig. 6. Sectioning procedure for HAZ-notched CTOD specimen according to API RP 2Z [11].

temperature, T_0 the inter-pass temperature and d_{HAZ} the distance between FL and HAZ line observed by macro-etching and assumed to be the A_{C3} boundary. In this work, A_{C3} is 968 K, obtained from dilatometry test [2], T_{mp} 1723 K, T_0 423 and 383 K for SMA- and SA-welded HAZ specimens, respectively, as listed in Table 2. From many studies [4–6,14,15], it has been established that an HAZ has four regions: coarse-grained HAZ (CGHAZ), fine-grained HAZ (FGHAZ), inter-critical HAZ (ICHAZ) with partially transformed microstructures and subcritical HAZ (SCHAZ) with tempered microstructures. A CGHAZ can be divided again into four characteristic zones according to the peak temperature of subsequent thermal cycles in a multi-pass welding procedure: (i) unaltered CGHAZ

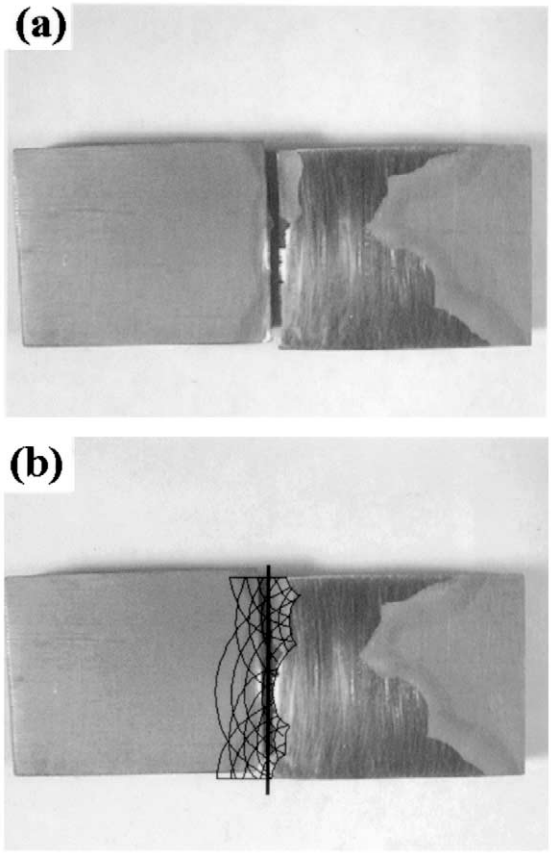

Fig. 7. Construction of microstructure-distribution map: (a) macro-etching of a specimen sectioned according to APR RP 2Z [11] (Fig. 6) and (b) indication of the thermal cycle history on the surface.

(UA CGHAZ), (ii) super-critically reheated CGHAZ (SCR CGHAZ), (iii) inter-critically reheated CGHAZ (IC CGHAZ) and (iv) subcritically reheated CGHAZ (SC CGHAZ). From a similar viewpoint, the microstructural classification listed in Table 3 was adopted in this investigation. The peak temperature was calculated by a conventional two-dimensional heat conduction analysis with the assumption that the temperature at the boundary of macro-etched HAZ is A_{C3} temperature [12]. The SCR CGHAZs and SC CGHAZs were roughly included in the FGHAZs and UA CGHAZs due to recrystallized fine grain size and similar fracture properties, respectively [2,3]. Finally, the microstructure-distribution map was completed by marking on it the locations of both the fatigue precrack and the crack initiation point (or points) observed on the fracture surface. Thus, analysis using the map has the advantage of being semi-empirical and systematic method because the map contains the experimental data d_{HAZ}, crack initiation point and precrack location. Microstructures sampled from arbitrary regions in the HAZs were found to be similar to the microstructures expected from the maps. Fig. 8 displays typical microstructures observed near the FL.

Table 3
Classification of microstructures in multi-pass welded HAZ adopted in this investigation

Peak temperature of first cycle (T_{p1})	Peak temperature of subsequent cycle (T_{p2})	Microstructure of HAZ
Melting point–1323 K (CGHAZ)	Melting point–1323 K	UA CGHAZ
	1323–968 K	SCR CGHAZ (FGHAZ)
	968–823 K	IC CGHAZ
	823–723 K	SC CGHAZ (UA CGHAZ)
	723 K–	UA CGHAZ
1323–968 K (FGHAZ)	Melting point–1323 K	UA CGHAZ
	1323–968 K	FGHAZ
	968–823 K	ICHAZ
	823 K–	FGHAZ
968–823 K (ICHAZ)	Melting point–1323 K	UA CGHAZ
	1323–968 K	FGHAZ
	968 K–	ICHAZ
823–723 K (SCHAZ)	Melting point–1323 K	UA CGHAZ
	1323–968 K	FGHAZ
	968–823 K	ICHAZ
	823 K–	SCHAZ

Fig. 9 shows the representative microstructure-distribution maps constructed from CTOD specimens tested at 111 K and used to confirm the existence of LBZ in the actual HAZ. Microstructures of possible LBZs at cryogenic temperatures, i.e. primarily IC CGHAZ and secondarily UA CGHAZ, are identified in front of the precrack tip, which was placed at FL or at FL+1 mm. As shown in the maps, there are three sorts of crack initiation points. In most cases near the FL, IC CGHAZs correspond to crack initiation points, as shown in Fig. 9(a). Secondly, when a relatively small fraction of an IC CGHAZ exists in front of the crack tip, an UA CGHAZ plays the role of the crack initiation point, as shown in Fig. 9(b). In some cases, the crack initiates not at the possible LBZ itself, but at the region near the LBZ, as shown in Fig. 9(c). The results of the first two situations are very compatible with those from simulated HAZ tests, which demonstrated that IC CGHAZs and UA CGHAZs are primary and secondary LBZs, respectively [3]. The third case can be explained by strength distributions in the crack tip front, as Suzuki et al. [13] discussed. According to their analysis, crack initiation near LBZ but not at LBZ itself, is induced by plastic constraint caused by LBZs, sometimes called local hard zones (LHZs) to emphasize their strength [6,13,16]. The local stress concentration and stress triaxiality of the constrained regions are elevated at times to the average stress in other regions so that a crack can initiate in a region near an LBZ. It can be concluded from the above results that the possible LBZs

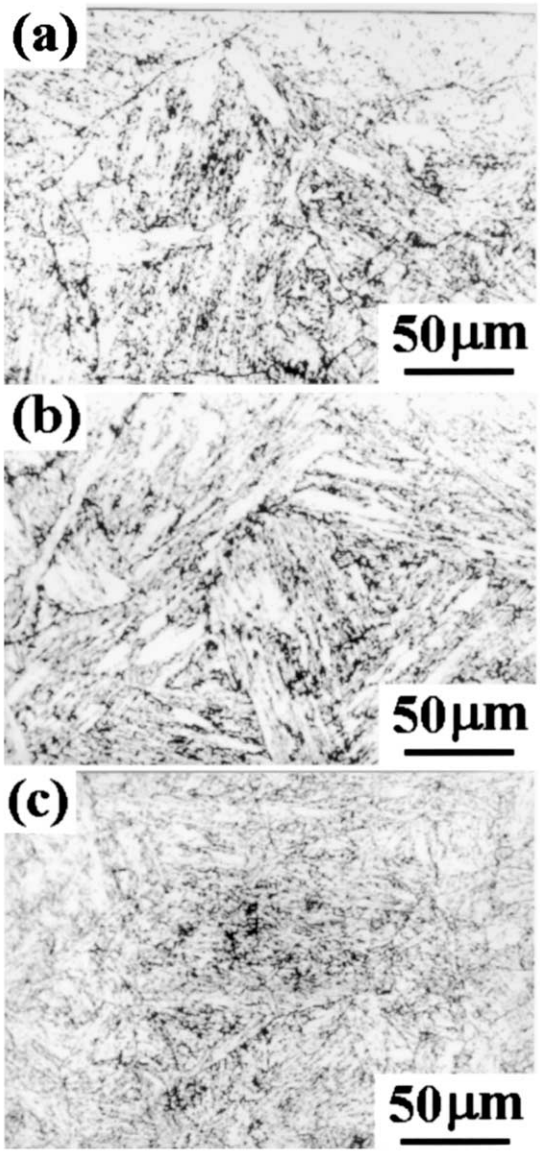

Fig. 8. Typical HAZ microstructures near FL observed in K-grooved HAZ specimens: (a) IC CGHAZ, (b) UA CGHAZ and (c) FGHAZ.

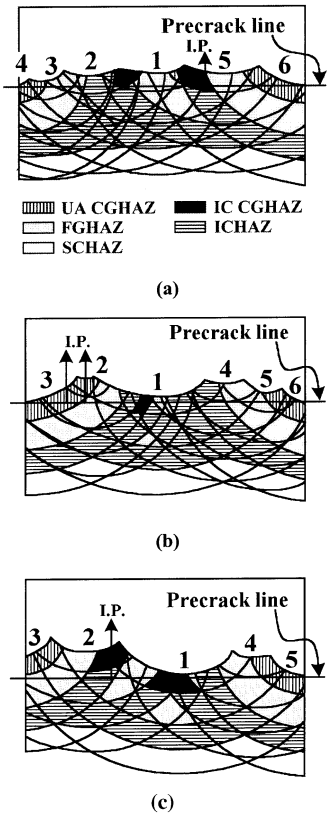

Fig. 9. Examples of HAZ microstructure-distribution maps used in this study (IP: crack initiation point, numbers: number of weld bead): (a) crack initiated at IC CGHAZ, (b) crack initiated at UA CGHAZ and (c) crack did not initiate at the possible LBZs.

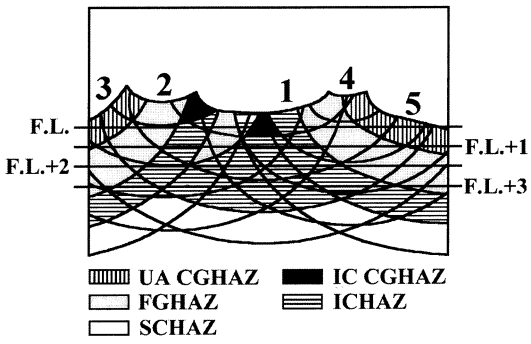

Fig. 10. An example of change in microstructure fraction according to precrack locations.

of this steel, i.e. primarily IC CGHAZs and secondarily UA CGHAZs as revealed in the previous work [3] using simulated HAZ specimens, are also the weak regions in the actual HAZs.

From the microstructure-distribution maps, one can also systematically derive a quantitative change in the microstructure fraction as a function of the distance from the FL, as shown in Fig. 10. Fig. 11 shows the fraction change in both SMA- and SA-welded joints, as measured on the maps and averaged. Comparison of Fig. 11 with Fig. 4 clarifies the fracture-controlling microstructures and modes. Generally, the fracture modes of materials with complex microstructures such as HAZs can be roughly divided into two types: weakest-link-type fracture and rule-of-mixture-type fracture [17]. In the areas around FL and FL+1 mm, there is a large fraction of FGHAZs, but the toughness values are much lower than those at FL+2 and +3 mm. This low toughness very likely arises because, as described above, the possible LBZs exist at those regions and cracks would preferentially initiate at them. The results indicate that the fracture behaviors at these regions are governed by the weakest-link-type fracture, not by the rule-of-mixture-type fracture. Conversely, the regions at FL+2 and +3 mm contain mainly two microstructures, i.e. FGHAZs and ICHAZs as shown in Fig. 10, and a negligible fraction of CGHAZs exists at

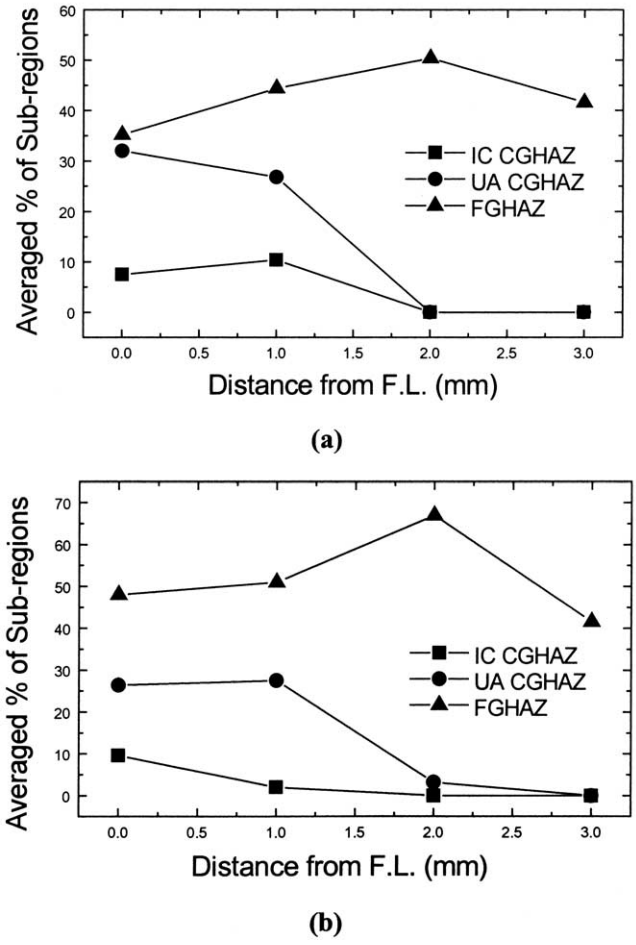

Fig. 11. Change in averaged fraction of subregions along distance from FL in (a) SA-welded and (b) SMA-welded joints.

the fatigue precrack front. Comparison of Fig. 11 with Fig. 4 shows that the line fraction of FGHAZs, the subregions with the highest toughness within HAZ due to grain size refinement, plays the main role in the toughness at the location. As a result, the toughness at FL+2 mm is higher than that at FL+3 mm due to the larger fraction of FGHAZ. Consequently, fracture in these regions is expected to be governed by a mixture-rule of the microstructures at the precrack tip front.

The relationship between the size of the LBZs, i.e. the total size of IC CGHAZs and UA CGHAZs, intersecting the precrack and the CTOD value was studied in order to determine the minimum fraction of LBZs necessary to initiate weakest-link-type fracture. Fig. 12 shows that the CTOD value decreases to its lowest level at 17% and remains unchanged as the size of the possible LBZ increases. It can be concluded that 17% is a critical fraction of CGHAZs that determines the fracture-type (weakest-link-type vs. rule-of-mixture-type). The results also provide a useful experimental criterion in the evaluation of the lower bound toughness in the QLT-steel HAZs: that HAZ-notched toughness tests should be performed using HAZ specimens in which the fatigue

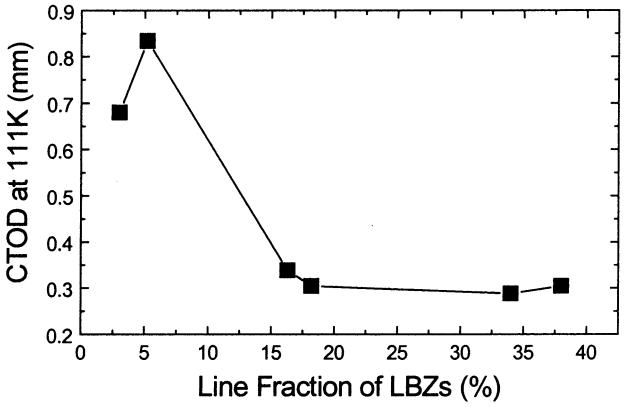

Fig. 12. Relationship between CTOD value and fraction of the LBZs (total fraction of IC CGHAZ and UA CGHAZ) at precrack tip front.

precrack intersects the CGHAZ over 17% of the precrack line fraction. Fig. 13 illustrates the microstructural influences on the actual HAZ toughness, summarizing all results obtained from the tests using K-grooved HAZ samples.

The experimental findings in this work elucidate the influences of the microstructure distribution on the cryogenic toughness within the actual HAZ of advanced 9% Ni steel. It is hoped that this study of metallurgical factors will be valuable in interpreting fracture characteristics in QLT-9% Ni steel HAZs, and thus in creating a better safety performance of LNG storage tanks. However, it should be noted that the metallurgical analysis is not a complete explanation of the HAZ fracture behaviors, since there are several important mechanical factors not taken into consideration, such as residual stress and strength mismatch between the weld metal and base metal. The authors are presently investigating the influence of such mechanical factors.

4. Conclusion

The correlation between the microstructure distribution and cryogenic fracture toughness in the actual

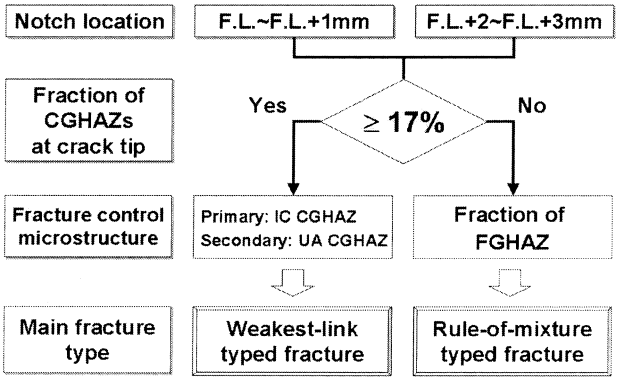

Fig. 13. Schematic diagram of fracture mechanism change according to precrack location.

HAZs of QLT-processed 9% Ni steel was investigated through CTOD tests using K-grooved HAZ specimens and microstructure-distribution maps drawn from the tested specimens. In the regions near the FL, the fracture behaviors were found to be dominated by weakest-link-type fracture because of the large fraction of LBZs (IC CGHAZ and UA CGHAZ), while in regions with LBZ fraction below 17% at the crack tip front, i.e. FL+2 and +3 mm, the fracture toughness was shown to be governed by the mixture-rule of microstructures at precrack tip front.

References

[1] C.H. Lee, S.W. Lee, J.Y. Yoo, W.Y. Choo, in: Proceedings of the Second Pacific Rim International Conference on Advanced Materials and Processing, Kyongju, Korea, 1995, pp. 2035–2044.
[2] J.-i. Jang, J.-B. Ju, W.-S. Kim, D. Kwon, J. Kor. Inst. Met. Mater. 38 (2000) 1001–1010.
[3] J.-i. Jang, B.-W. Lee, J.-B. Ju, D. Kwon, W.-S. Kim, Mater. Sci. Eng. A 340 (2003) 68–79.
[4] B.C. Kim, S. Lee, N.J. Kim, D.Y. Lee, Metall. Trans. A 22 (1991) 139–149.
[5] D.P. Fairchild, Fatigue and Fracture Testing of Weldments, ASTM STP 1058, American Society for Testing and Materials, Philadelphia, PA, 1990, pp. 117–141.
[6] M. Toyoda, J. Jpn. Weld. Soc. 62 (1993) 603–616.
[7] ASTM Standard E 1290, Standard Test Method for Crack-Tip Opening Displacement (CTOD) Fracture Toughness Measurement, American Society for Testing and Materials, 1993.
[8] K. Satoh, M. Toyoda, F. Minami, S. Satoh, M. Nakanishi, K. Arimochi, J. Jpn. Weld. Soc. 52 (1983) 154–161.
[9] J.-i. Jang, Y.-C. Yang, W.-S. Kim, D. Kwon, Adv. Cryog. Eng. 44 (1998) 41–48.
[10] J.-i. Jang, Y.-C. Yang, W.-S. Kim, D. Kwon, Met. Mater. Int. 3 (1997) 230–238.
[11] API RP 2Z, 2nd ed., Recommended Practice for Preproduction Qualification for Steel Plates for Offshore Structures, American Petroleum Institute, 1992.
[12] Y. Nakao, H. Oshige, S. Noi, Quart. J. Jpn. Weld. Soc. 3 (1985) 767–773.
[13] S. Suzuki, K. Bessyo, M. Toyoda, F. Minami, Quart. J. Jpn. Weld. Soc. 13 (1995) 302–308.
[14] S. Lee, B.C. Kim, D. Kwon, Metall. Trans. A 23 (1992) 2803–2816.
[15] C.L. Davis, J.E. King, Metall. Trans. A 25 (1994) 563–573.
[16] F. Minami, H. Jing, M. Toyoda, F. Kawabata, K. Amono, IIW Document X-1254-92, 1992.
[17] M. Toyoda, J. Jpn. Weld. Soc. 59 (1990) 166–172.